# Comparison of Semi-Empirical Single Point Wall Pressure Spectrum Models with Experimental Data

**Nicholas Thomson and Joana Rocha ***

Department of Mechanical and Aerospace Engineering, Carleton University, 1125 Colonel By Drive, Ottawa, ON K1S 5B6, Canada; NickThomson@cmail.carleton.ca
\* Correspondence: Joana.Rocha@carleton.ca

**Abstract:** This study presents an evaluation of semi-empirical single-point wall pressure spectrum models by comparing model predictions with wind tunnel and flight test data. The mean squared error was used to compare the power spectral density of the wall pressure fluctuations predicted by semi-empirical models with a large amount of experimental data. Results show that the models proposed by Goody and Smol'yakov have the lowest mean squared error when predicting the power spectral density for wind tunnel experiments and the Rackl and Weston model has the lowest mean squared error when predicting the power spectral density for flight test data. In addition, although current studies of the power spectra obtained in the wind tunnel are similar, they are not generally an accurate representation of flight test experiments.

**Keywords:** aeroacoustics; turbulent boundary layer; scaling; acoustics; modelling

## 1. Introduction

Pressure fluctuations caused by the turbulent boundary layer (TBL) in fluid flows are a source of noise and vibration. These surface pressure fluctuations may cause problems such as structure fatigue and the generation of acoustic noise radiation [1]. Controlling TBL pressure fluctuations and limiting radiated noise can reduce excess noise within the cabin of aircraft, acoustic interference in communication, the malfunction of sensitive equipment, and adverse health effects [2,3].

There have been many studies over the years on determining and describing the sound generated in the TBL to better understand, predict, and possibly control it. Bull provides a good summary of the different studies on the subject [1]. In 1962, Willmarth and Wooldridge were the first to comprehensively measure the pressure fluctuations in the turbulent boundary layer of a wind tunnel by placing pressure transducers flush with the flow through the test section [4]. They were also the first to notice that the power spectral density (PSD) of the wall pressure fluctuations was found to scale with certain flow parameters such as the free stream velocity and the boundary-layer displacement thickness. They found that the energy density of the wall pressure fluctuations was highest at low frequencies and that it decayed with higher frequencies. They also showed that a small increase in surface roughness causes a profound effect on the fluctuating wall pressure in the immediate vicinity. Farabee and Casarella later showed that the PSD is separated into four regions; a low frequency, medium frequency, overlap, and high-frequency range, as confirmed by Bull [5]. The low frequency range is defined as $\omega\delta/u_\tau < 5$, the medium frequency as $5 < \omega\delta/u_\tau < 100$, the high region as $\omega v/u_\tau^2 < 0.3$, and the overlap region is defined as the region between the medium frequency region and the high frequency region. The distinct frequency regions are often used to describe the PSD since they have distinct power-law features, and the approximate slope of the pressure spectrum in these regions is the common method for comparing experimental data. The slope measured for each region from different studies was tabulated by Blitterswyk [6].

Since Bull, there have been several new wind tunnel studies performed on wall pressure fluctuations, such as by Goody and Simpson [7], Blitterswyck and Rocha [8], Miller [9] and Salze et al. [10], as well as flight test experiments from the National Aeronautics and Space Administration (NASA), using a Tuplov 144 [11] and a Gulfstream G550 [12], which include PSD data. The flight test data were obtained in both experiments by mounting an array of microphones flush with the fuselage of the aircraft, and then measuring the surface pressure fluctuations at different altitudes and velocities.

TBL PSD models are used by researchers to compare with individual experiments, generally, one at a time, to verify whether the obtained experimental data are in good agreement with experimental work previously done, as found in the literature. The present work compares how several TBL PSD wall pressure fluctuation models predict some of these experiments and investigates which model is the most reliable in its predictions of the PSD, as well as when certain models are preferable. Another key contribution of the current study is the comparison between models designed from wind tunnel experiments and models designed from flight tests. The models compared in this study are Efimtsov [13–15], Rackl and Weston [11,15], Lowson [16], Robertson [17], Lagnelli [18], Goody [19] and Smol'yakov [20].

Studies by Hwang et al. [21] and Blittersyck and Rocha [6,8] have compared existing semi-empirical models used to describe the acoustic response. Blittersyck and Rocha found that models by Efmitsov, and Rackl and Weston best predicted the low to medium frequency; while models by Goody and Smol'yakov best predicted the overlap and high-frequency ranges. The work by Hwang et al. concluded that Goody provided the best overall prediction of the pressure spectra for flows in air and water [21].

## 2. Materials and Methods

### 2.1. Data

The different experimental PSD datasets sampled are in Figures 1 and 2 and are scaled on the inner and outer boundary layer variables, respectively. The naming convention used in the figures and tables is the name of the first researcher presented in the paper, followed by the momentum thickness Reynolds number, and by either a "w" denoting a wind tunnel, or "f" for a flight test. The boundary layer variables used to scale the experimental data are in Table A1 in Appendix A.

Scaling is based on the concept of self-similarity and is done to describe the boundary layer shape over different conditions, collapsing the data into a similar range with other experiments [1,19]. When scaled on the inner variables, the different wind tunnel datasets collapsed to show general agreement between each other, including a good collapse in the high-frequency range. It is pertinent to note how the flight test PSD data from the Tu144 experiment by Rackl, Rizzi and Andianov [11] and the Gulf Stream PSD data by Rocha and Palumbo [12] collapse with each other but not with the wind tunnel data. This is somewhat unexpected since Miller [9] performed an experiment at a similar Mach number and Reynolds number in the wind tunnel as the flight test for Rocha239216f; however, the Miller data collapsed with the other wind tunnel experiments and Rocha239216f did not. Some variation between wind tunnel and flight test data is expected since wall pressure fluctuations in the wind tunnel are observed for controlled conditions with known roughness and pressure gradients. Flight test data can be subject to error since the boundary layer can be disturbed by rivets and have pressure gradient fluctuations [3]. Wind tunnel experiments also tend to have a smaller boundary layer, as the length for the boundary layer to develop is restricted by the size of the test section, whereas for a flight test the boundary layer begins at the nose of the aircraft. The high-frequency ranges do not collapse well when scaled on outer boundary layer variables, this is expected since the high-frequency range is caused by small inner boundary layer vortices and because a wide range of different transducers was used. Experiments with a small $d^+$ do not properly capture the high-frequency roll-off due to attenuation, this causes the slope of the roll-off to increase.
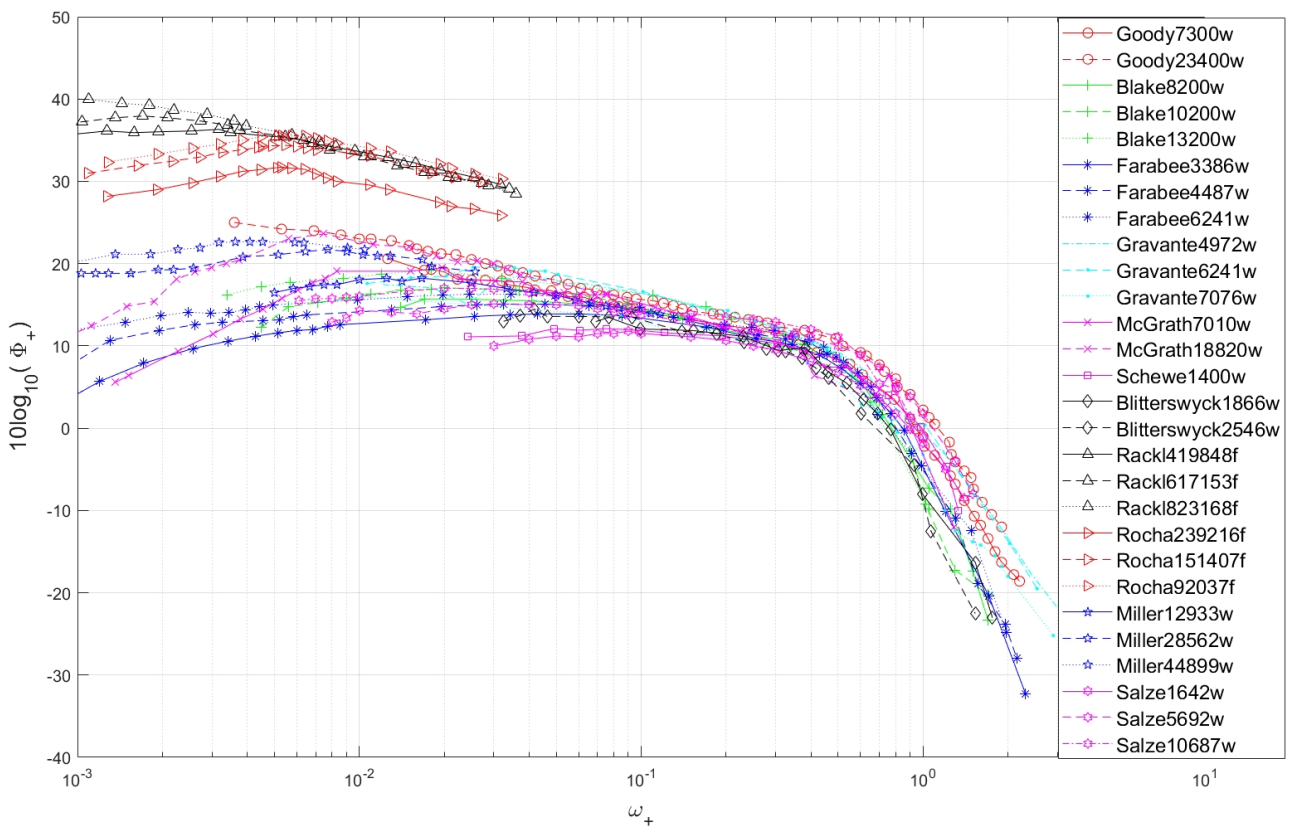
**Figure 1.** Experimental pressure spectra scaled on inner variables.
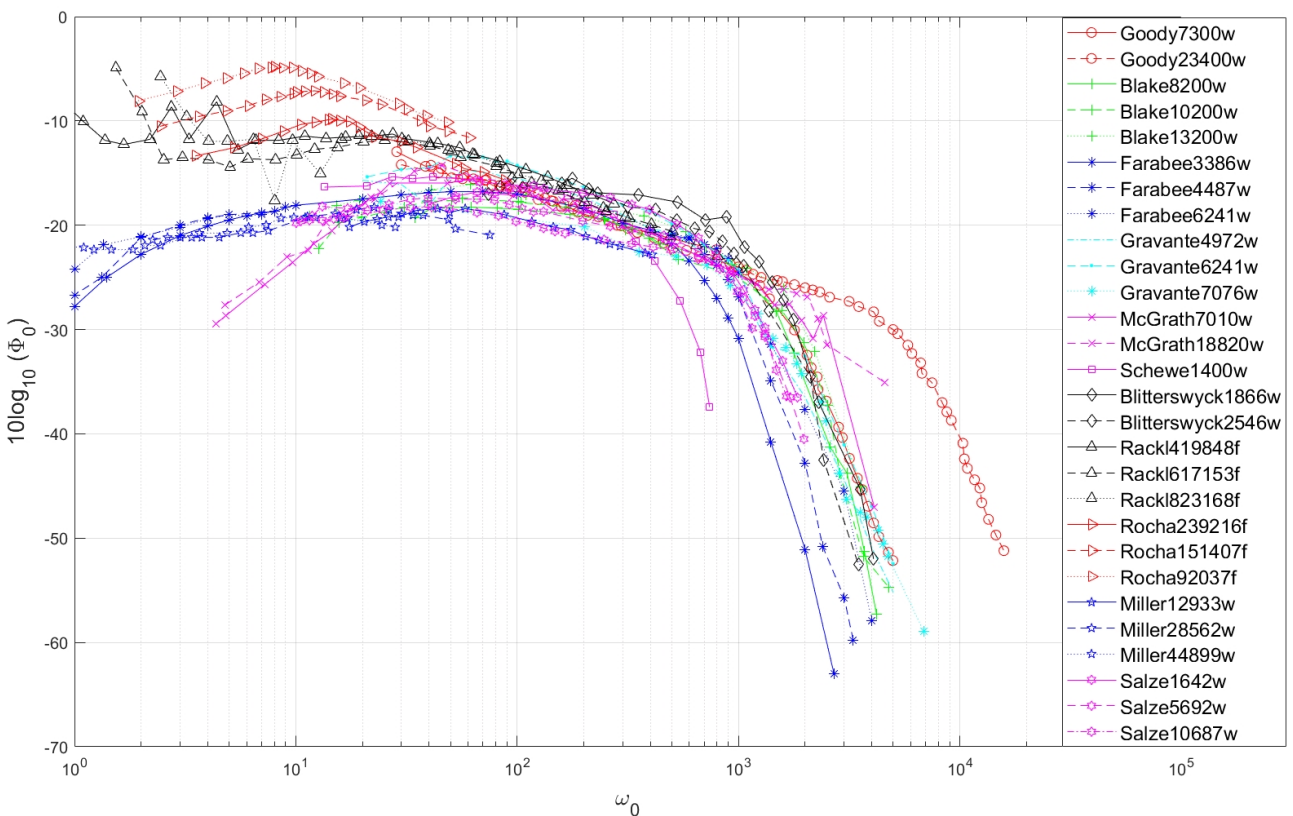


**Figure 2.** Experimental pressure spectra scaled on outer variables.

Each of these studies made different design choices to have a fully developed boundary layer. Schewe [22], Goody and Simpson [7], and Blake [23] allowed the flow to develop naturally into a fully developed boundary layer, whereas Farabee and Casarella [24], McGrath and Simpson [25], Gravante et al. [26] and Blitterswyk and Rocha [8] used either trip wires or sandpaper strips to artificially trip the flow into a fully developed turbulent boundary layer. A fully developed boundary layer causes the flow conditions to become steady and predictable with increased stream-wise distance, ensuring accurate prediction and repeatability in experiments. The wind tunnel data compared in this study are for a zero pressure gradient, two-dimensional flow, with a single-sided power spectrum.

Each of the experiments must contend with two issues concerning measuring the PSD. At low frequencies, there is often background noise that contaminates the data. At high frequencies, there is attenuation caused by the finite size of the microphone. Anechoic chambers and noise filtering techniques have been used to correct background noise. Anechoic chambers absorb the noise radiated outward and prevent it from reflecting, as well as absorbing noise from outside the test section from entering the chamber and contaminating the data [27]. Anechoic chambers were used by Blake, Farabee and Casarella, Schewe, and Blitterswyck and Rocha. Noise cancellation techniques can also be used to reduce undesired noise. A common approach to filtering out background noise is a temporal subtraction of two spanwise transducer signals that can be assumed to be uncorrelated by having them separated by a couple of boundary layer thicknesses [28,29]. Noise cancellation techniques were used by Farabee and Casarella, Gravante et al., Goody and Simpson, McGrath and Simpson, Blitterswyck and Rocha, and Miller.

The size of the microphone used has a significant impact on the ability to measure high-frequency noise. If the contribution to the pressure fluctuation from a source is smaller than the sensing diameter of the transducer then it will be attenuated, effectively acting as a low-pass filter. This is caused by the contribution of the source being spatially integrated and sources smaller than the sensing diameter are attenuated since their mean value will be zero by definition [26,30]. It was shown by Schewe [22] and Gravante [26] that the effective size of the pressure transducer to reduce attenuation should be $12 < d^+ < 19$. A way to reduce the effective size is to use a pinhole capped microphone as opposed to a grid capped microphone.

Another way to reduce high-frequency attenuation is by applying the Corcos correction [31]. This is a table that can be used to try to recover high-frequency spectral values and has been shown to have favorable results in several studies. Nevertheless, other studies have raised concerns that the Corcos correction can lead to over correction at high frequencies [22,30]. Since it is unclear when it is appropriate to apply the Corcos correction, the data in this work are as reported by the original authors of each study.

Several of the authors sampled in this study commented on the uncertainty of hotwire measurements for TBL parameters and on the uncertainty of microphone measurements. TBL parameters' measurements, such as mean velocity, had a low uncertainty of approximately 1–3% as measured by McGrath and Simpson, and Blake. Goody and Simpson, Blake, McGrath and Simpson, Rocha and Palumbo, and Gravante et al. commented on the uncertainty of the microphones in their experiments, in which the amount of uncertainty was between 1–3 dB. Rocha and Palumbo, and Gravante et al. also commented on how the uncertainty varied with frequency range. Gravante et al. found that the uncertainty of the measured turbulent wall pressure spectra was highest above 10,000 Hz where it was approximately 7%. Miller, Salze, Schewe, Farabee and Casarella did not mention uncertainty; however, they used similar instrumentation as the other authors, and so it would be reasonable to hypothesize that uncertainty is also low.

## 2.2. Single Point Wall Pressure Spectrum Models

Single point wall pressure spectrum semi-empirical models have been used to predict the PSD of wall pressure fluctuations for zero pressure gradient flows. By using the TBL parameters measured in wind tunnels and flight tests as input parameters to the TBL

semi-empirical models, the PSD of the wall pressure fluctuations can be predicted. These models are generally constructed by using the observed scaling behavior of existing data as a starting form, and then by adjusting the constants of those scaling parameters to better match the existing data. This section describes each of the TBL semi-empirical models used in the present investigation. The single-sided PSD is defined as follows:

$$\bar{p^2} = \int_0^\infty \Phi(\omega) d\omega \tag{1}$$

$$\Phi(f) = 2\pi\Phi(\omega), [pa^2, Hz] \tag{2}$$

$$PSD = 10log_{10}(\frac{\Phi(f)}{P_{ref}^2}), [DB] \tag{3}$$

in which $\Phi(\omega)$ is the single point wall pressure spectrum, either provided by the respective TBL semi-empirical model or from the experimental data.

### 2.2.1. Efimtsov Model

Efimtsov created two models from flight tests using a Tupolev TU-22 (Soviet twin-engined, supersonic military aircraft) and additional wind tunnel experiments [13–15]. According to Efimtsov, a single point wall pressure spectrum model should be based around Mach Number, Reynolds number, and Strouhal number. The second of Efimtsov's equations is shown in Equation (1).

$$\Phi(w) = \frac{2\pi\alpha u_\tau^3 \rho^2 \delta\beta}{(1 + 8\alpha^3(\frac{\omega\delta}{u_\tau})^2)^{1/3} + \alpha\beta Re_\tau((\frac{\omega\delta}{u_\tau})/Re_\tau)^{10/3}}, \tag{4}$$

where:

$$Re_\tau = \frac{\delta u_\tau}{v_w} \tag{5}$$

$$\beta = [1 + (\frac{Re_{\tau 0}}{Re_\tau})^3]^{1/3} \tag{6}$$

$$\alpha = 0.01, \tag{7}$$

$$v_w = v\frac{\rho}{\rho_w}(\frac{T_w}{T})^{0.89} \tag{8}$$

$$T_w = T(1 + 0.89\frac{\gamma - 1}{2}M^2) \tag{9}$$

$$\rho_w = \rho\frac{T}{T_w}. \tag{10}$$

### 2.2.2. Rackl and Weston

Rackl and Weston used data collected from a TU144 to adjust Efimtsov to better predict a broadband peak around a Strouhal number of 0.6 and to adjust the high-frequency roll-off of the PSD. They did this by creating two semi-empirical corrective functions that add to the Efimtsov model [11,15].

The equation becomes:

$$\Phi(f) = \Phi(f)_{Efimtsov} + x_1(f) + x_2(f), \tag{11}$$

where the corrective functions are:

$$x_1(f) = 1/4[tanh(log_{10}(\frac{f}{1000})) + 1][M - 1.65]log_{10}(f) \tag{12}$$

$$x_2(f) = 2.5e^{(-(ln(\frac{2\pi\delta^*}{U_\infty}(f)) - ln(0.6))^2)}. \tag{13}$$

### 2.2.3. Lowson Model

The semi-empirical model developed by Lowson was done for both supersonic and subsonic equilibrium boundary layers and tries to relate the power spectral density (PSD) to the Mach number and other TBL parameters [16]. This model was intended to be used directly for structural response calculations with the goal of being simple, related to physical parameters of the flow, and having a good agreement with available data.

$$\Phi(f) = \frac{q^2(\frac{\bar{P}2}{q^2})}{\omega_0(1 + (\frac{2\pi f}{\omega_0})^2)^{3/2}}, \tag{14}$$

where:

$$\omega_0 = \frac{8U_\infty}{\delta} \tag{15}$$

$$\frac{\bar{P}2}{q^2} = \frac{0.006^2}{(1 + 0.14M^2)^2}. \tag{16}$$

### 2.2.4. Robertson Model

Robertson built on Lowson to try to improve upon the high-frequency roll-off and an overestimation of the low-frequency range [17]. This model was intended to be used for aerospace vehicles such as the space shuttle and a major portion of the investigation Robertson performed was for transonic speed conditions and the launch phase of the shuttle's mission ($0.60 \le M \le 1.6$).

$$\Phi(f) = \frac{q^2(\frac{\bar{P}2}{q^2})}{\omega_0(1 + (\frac{2\pi f}{\omega_0})^{0.9})^2}, \tag{17}$$

where:

$$\omega_0 = \frac{U_\infty}{2\delta^*}. \tag{18}$$

### 2.2.5. Lagnelli Model

Through further subsonic and supersonic wind tunnel tests, Lagnelli proposed a further update of Robertson. Lagnelli accounts for viscous, compressibility and wall heat transfer effects and is based on the work by Lowson, Robertson and Blake [18]. Based on the availability of information, the ratio of $h_w/h_{aw}$ was assumed to be unity in this study. While this assumption has little effect for low Mach number flows, it leads to error at higher Mach numbers.

$$\Phi(f) = \frac{q^2\delta^*(2.293 \times 10^{-5})F_c^{-0.5733}}{U_\infty[1 + F_c^{2.867}(\frac{2\pi f\delta^*}{U_\infty})^2]}, \tag{19}$$

where $F_c$ is a transformation function for compressible to compressible flow states.

$$F_c = \frac{1}{2} + \frac{h_w}{h_{aw}}(\frac{1}{2} + (0.89)\frac{\gamma - 1}{2}M^2) + 0.22(0.89)\frac{\gamma - 1}{2}M^2. \tag{20}$$

### 2.2.6. Goody Model

Goody decided to modify the Chase–Howe model [32,33] based on experimental data from Goody and Simpson [7], Farabee and Casarella [24], Gravante et al. [26], McGrath and Simpson [25], Olivero-Bally et al. [34] and Blake [23]. The Goody model tries to improve the Chase-Howe model in the prediction of the low-frequency response and the roll-off at high frequencies. This was done by adding a term to the denominator so that the spectral levels decay at $\omega^{-5}$, changing exponents in the denominator to better agree at middle frequencies,

and adding a multiplicative constant to raise the spectral levels at all frequencies to better agree with the experimental data.

$$\Phi(f) = \frac{3(2\pi f \tau_w)^2 (\frac{\delta}{U_\infty})^3}{((\frac{2\pi f \delta}{U_\infty})^{3/4} + 0.5)^{3.7} + (1.1 R_T^{-0.57} \frac{2\pi f \delta}{U_\infty})^7}. \tag{21}$$

### 2.2.7. Smol'yakov Model

Smol'yakov used several datasets to create a piece wise function model that has different equations for the low, overlap and high frequency ranges [20]. The method is based on modelling of the wave-number spectrum of the sources caused by the interaction of the turbulence–mean shear type.

$$\Phi(f) = \frac{1}{u_\tau^2} 1.49 x 10^{-5} \tau_w^2 \nu Re_\theta^{2.74} \bar{f}^2 (1 - 0.117 Re_\theta^0 .44 f^{\bar{1}/2}), \tag{22}$$

for $\bar{f} < \bar{f}_0$

$$\Phi(f) = \frac{2.75 \tau_w^2 \nu}{u_\tau^2 \bar{f}^{1.11}} (1 - 0.82 exp[-0.51(\frac{\bar{f}}{\bar{f}_0} - 1)]), \tag{23}$$

for $\bar{f}_0 < \bar{f} < 0.2$

$$\Phi(f) = \frac{\tau_w^2 \nu (3.89 exp(-8.35\bar{f} + 18.6 exp(-3.58\bar{f}) + 0.31 exp(-2.14\bar{f}))}{1 - 0.82 exp(-0.51(\frac{\bar{f}}{\bar{f}_0} - 1))} \tag{24}$$

for $\bar{f} > 0.2$ where:

$$\bar{f} = \frac{2\pi f \nu}{u_\tau^2} \tag{25}$$

$$\bar{f}_0 = 49.35 Re_\theta^{-0.88}. \tag{26}$$

## 3. Results and Discussion

The comparison between models and the different experiments was done by determining the mean squared error (MSE) between the PSD of the wall pressure fluctuations predicted by the semi-empirical single point models and the PSD of wall pressure fluctuations measured in each of the experiments. The MSE is then defined for this application as follows:

$$MSE = \frac{1}{N} \sum_{n=1}^{N} (PSD_{experimental,n} - PSD_{predicted,n})^2, \tag{27}$$

in which $n$ is the PSD sampled at a specific frequency, and N is the total number of samples taken. In previous studies found in the literature, the evaluation of models and experiments are made either by visual inspection or by comparing the slope of the PSD for the low, medium, overlap and high-frequency ranges. Comparing the models based solely on the slope of PSD at different frequencies fails to account for a difference in magnitude. Ideally, both the shape and magnitude of the PSD should be compared when evaluating a model so that accurate estimations of the sound produced can be determined. The PSD for Goody23400w and Rackl419848f can be seen in Figures 3 and 4, respectively, along with the semi-empirical model predictions for the same flow conditions. From visual inspection of Figure 3, it is not apparent which model best describes Goody23400w. However, it can be seen by looking at the MSE that the Goody model has the lowest MSE with 1.3 closely followed by the Smol'yakov model with 8.9, while the Efimtsov and Rackl and Weston models perform poorly. For the Rackl1419848f, the Rackl and Weston model has the lowest MSE, followed by the Efimtsov model, while the Goody and Smol'yakov models perform poorly, as seen in Figure 4.

The MSE of the PSD between each model and experiment is shown in Appendix B in Table A2. The MSE of the PSD at different frequency ranges is also included in Appendix A to show how the models performed in certain ranges. Table A3 is the MSE for the low-frequency range, Table A4 is the medium frequency range, Table A5 is the overlap range, and Table A6 is the high-frequency range.
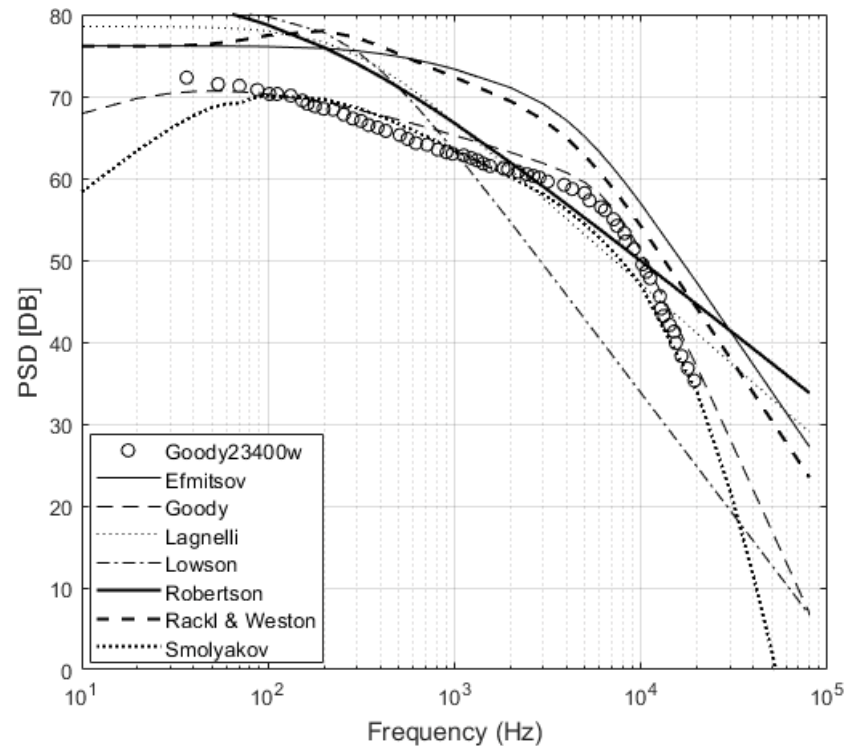


**Figure 3.** Goody23400w compared to models, MSE for each model: Efimtsov 74.9, Goody 3, Lagnelli 27.3, Lowson 114.1, Robertson 28.1, Rackl and Weston 60.3, Smol'yakov 4.1.

Except for Goody, the PSD compared in this report does not provide an accurate prediction of the low-frequency range. The low-frequency range is a difficult range for experiments to capture due to noise from the fan and structural vibration leading to a contamination of the data. An increase seen in the pressure spectrum below 10 Hz can also be the result of pressure fluctuations from the irrotational motion of the flow above the boundary layer [24]. Farabee and Casarella had a significant amount of experimental data in the low-frequency range and were used in the creation of the Goody model [19].

The mid-frequency range and the overlap frequency range are well predicted and have a low MSE between the models and the experiments. This can be attributed to this being the range where the majority of data points were taken during experiments and therefore used in the creation of the models.

The high-frequency range is a function of the inner variables of the boundary layer and should be scaled based on the viscosity as the inner region is dominated by viscous forces. The difficulty in this region is that frequency attenuation is problematic for obtaining reliable data. Focusing on Gravante, Schewe, Blitterswyck and Salze1642w as the studies with the smallest $d^+$, the MSE is much smaller when compared to each model, and the Goody and Smol'yakov models have the lowest MSE. This is expected as Schewe demonstrated how a larger $d^+$ causes a steeper roll-off of the high-frequency response [22].
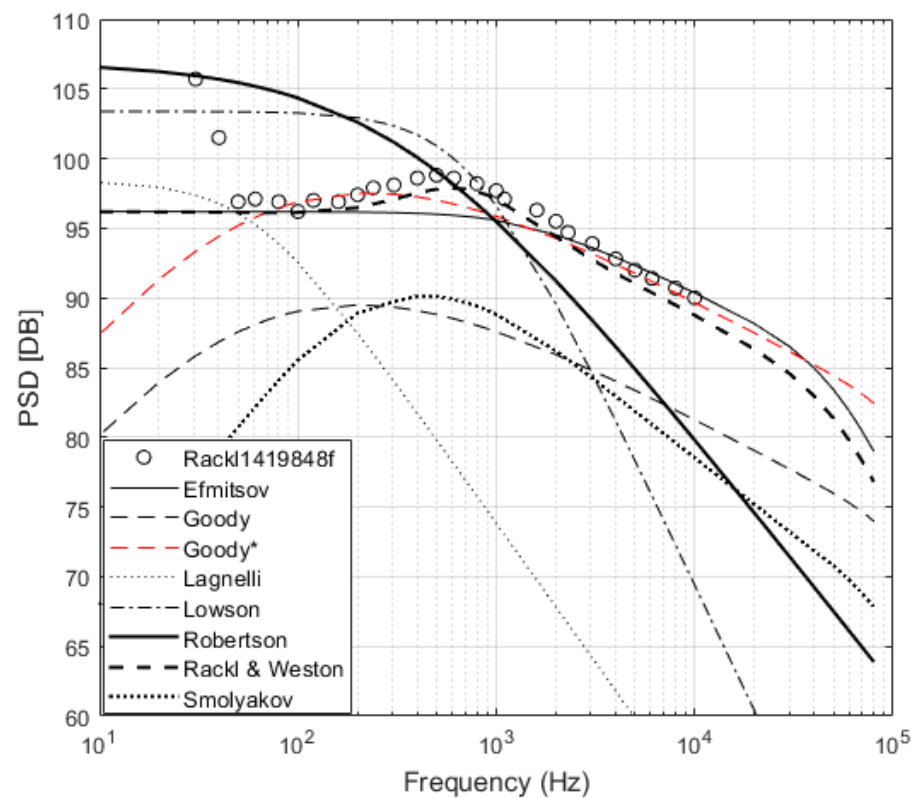
**Figure 4.** Rackl419848f from Tu144 window bank 4 compared to models, MSE for each model: Efimtsov 8.1, Goody 117.1, Goody* 8.9, Lagnelli 234.1, Lowson 41, Robertson 25.8, Rackl and Weston 7.5, Smol'yakov 201.1.

The results show that the models proposed by Efimtsov [14] and Rackl and Weston [15] both performed well when compared to the flight test PSD measurements, but poorly when compared to the PSD measured in wind tunnel experiments. Furthermore, when comparing against all the different data sets, the model proposed by Rackl and Weston consistently outperforms the model by Efimtsov, which indicates that the changes added to the Efimtsov model by Rackl and Weston better represent the PSD.

The models proposed by Goody [19] and Smol' yakov [20] have the lowest MSE when predicting the PSD. However, when compared to the flight test data they did not perform as well. It is worth noting that when Goody and Smol'yakov proposed their respective models they postulated these would be effective even at high Reynolds numbers. This is confirmed from the comparison of their models to the experiments by Miller. Goody and Smol'yakov both predict the shape of the PSD from the flight tests well, with a decay of the overlap region being approximately $\omega^{-0.7}$, meaning that an adjustment only needs to be made to the magnitude.

The initial functional form of the Goody model is [19]:

$$\Phi(f) = \frac{C_2(2\pi f \tau_w)^2 (\frac{\delta}{U_\infty})^3}{((\frac{2\pi f\delta}{U_\infty})^{3/4} + C_1)^{3.7} + (C_3^{-0.57}\frac{2\pi f\delta}{U_\infty})^7},$$

(28)

with parameters $C_1$, $C_2$, and/or $C_3$ varying with the Reynolds number. $C_1$ and $C_3$ determine the slope of the low and high frequency ranges, respectively, and also determine the size of the overlap region. $C_2$ acts as a multiplicative constant that increases the spectral levels at all frequencies so that the model better agrees with experimental data. Goody used the values $C_1 = 0.5$, $C_2 = 3.0$ and $C_3 = 1.1R_T^{-0.57}$ to agree with a selection of wind tunnel experiments.

To update the Goody model to fit the flight test pressure spectra data in this study, the parameters were modified to $C_1 = 0.55$ and $C_2 = 21$, as displayed in red in Figures 4–6. These values provide a local minimum for the MSE between the Goody model and the flight test experiments, the results of which are comparable to Efimtsov and Rackl and Weston. To create a universal model for flight test PSD, a $C_2$ parameter that scales effectively would be desirable. Goody suggested that $C_2$ should scale on the Reynolds number; however, Goody predicted Miller44899w well but not Rocha239216f, which has a similar Reynolds number. The adjusted Goody model does well predicting the magnitude and the shape of the pressure spectra for the four flight test experiments that are near Mach 0.7, as can be seen in Figures 4 and 5. However, the adjusted Goody model overpredicts Rocha239216f, which is at a lower Mach number, and underpredicts Rocha92037f, which is at a higher Mach number, as shown in Figure 6. This suggests that a $C_2$ scaling parameter should include a velocity component as well. Other possible scaling parameters are the shear velocity and momentum thickness, given that the flight test data display much higher values for these parameters than the wind tunnel PSD data. However, currently there are not enough variety in high-speed and flight test PSD experiments to define a clear trend.

The findings from this study support that future work needs to be undertaken to improve current wall pressure fluctuation PSD prediction. Further high-speed wind tunnel and flight test experiments should be undertaken to better determine what factors cause the appearance of a broadband peak, and also to improve the understanding of the differences between wind tunnel and flight test experiments.
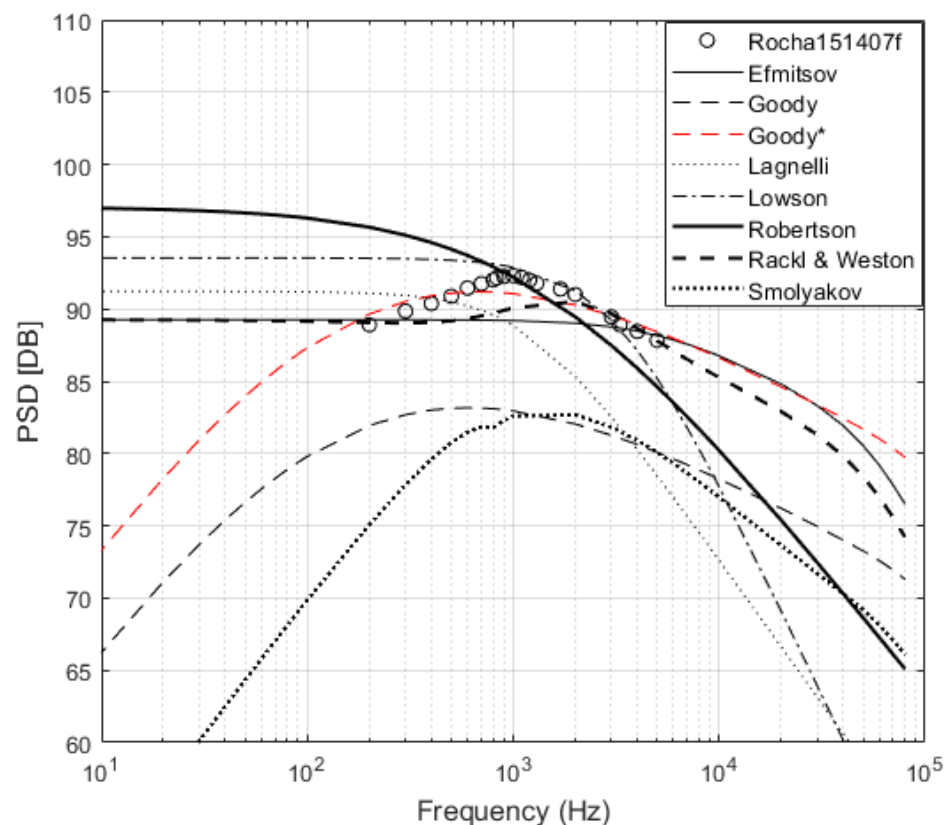


**Figure 5.** Rocha151407f compared to models, MSE for each model: Efimtsov 4.4, Goody 71.5, Goody* 0.6, Lagnelli 21.1, Lowson 3.6, Robertson 7.3, Rackl and Weston 2.4, Smol'yakov 93.3.
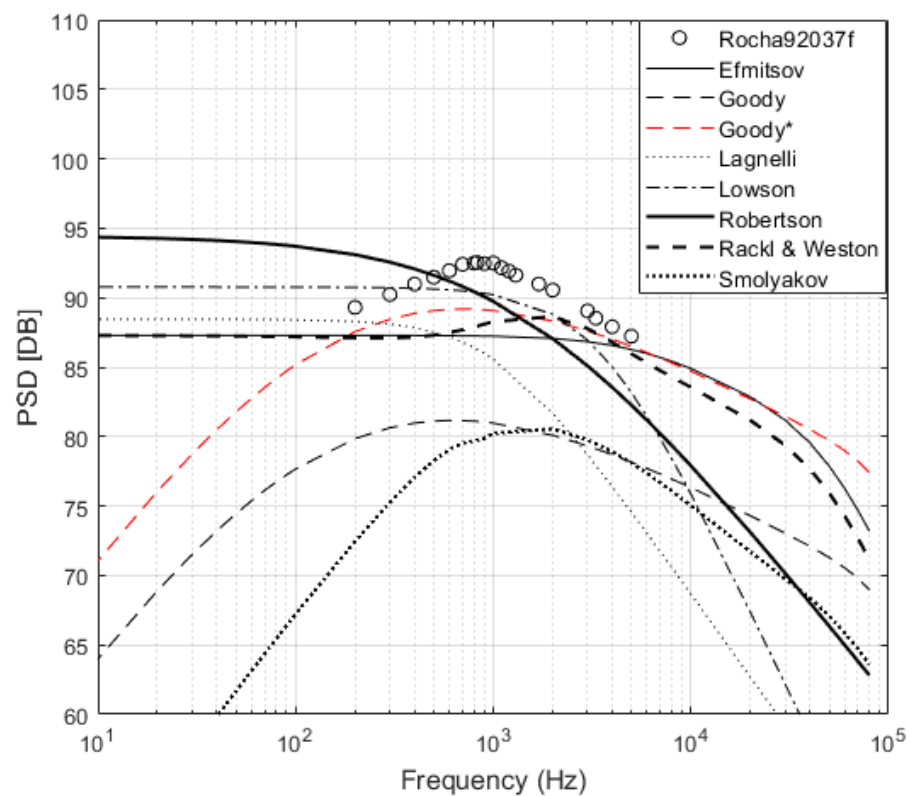
**Figure 6.** Rocha92037f compared to models, MSE for each model: Efimtsov 16.1, Goody 110.3, Goody*
6.4, Lagnelli 56.1, Lowson 4.1, Robertson 8.8, Rackl and Weston 11.4, Smol'yakov 145.5.

## 4. Conclusions

Existing semi-empirical models have been compared with experimental flight tests
and wind tunnel data to better understand what methods of prediction are effective
for determining the wall pressure fluctuation PSD. The MSE of the PSD between semi-
empirical models and experimental data has been proposed as a comparison method since
it provides insight into the effectiveness of the existing models. It was found that existing
flight test and wind tunnel data do not collapse with each other for the same scaling values,
and the best models for predicting the PSD for flight test and wind tunnel experiments
are not the same. Goody or Smol'yakov are more accurate for the prediction of wind
tunnel results or the for the validation of wind tunnel results. Rackl and Weston are more
accurate for the prediction of in-flight PSD. This study also shows that Goody could be
altered to better predict flight test PSD; however, a universal scaling parameter still needs
to be found. Further high-speed wind tunnel testing is required to better represent the
results measured from flight tests and to improve the prediction of existing wall pressure
fluctuation PSD models. The authors are in the process of performing wind tunnel testing
to better understand the inaccuracies of existing semi-empirical models and to improve the
accuracy of PSD predictions.

### Nomenclature

The following nomenclature is used in this manuscript:

| | |
|---|---|
| $d$ | pressure transducer diameter, [m] |
| $d^+$ | $d$ normalized by viscous length scale $u_\tau d/\nu$, nondimensional |
| $f$ | frequency, [Hz] |
| $p$ | pressure fluctuation at the surface, [pa] |
| $q$ | dynamic pressure $1/2\rho U_\infty^2$, [pa] |
| $Re_x$ | Reynolds number based on streamwise distance $\frac{U_\infty x}{\nu}$, nondimensional |
| $Re_\theta$ | Reynolds number based on momentum thickness $\frac{U_\infty \theta}{\nu}$, nondimensional |
| $U$ | velocity at the edge of the boundary layer, [m/s$^2$] |
| $\nu$ | kinematic viscosity of air, [$m^2/s$] |
| $\tau_w$ | Shear stress at the wall, [pa] |
| $u_\tau$ | friction velocity, $(\tau_w/\rho)^2$ [m/s$^2$] |
| $\rho$ | mass density of flow, [kg/m$^3$] |
| $\delta$ | boundary layer thickness, [m] |
| $\theta$ | boundary layer momentum thickness, [m] |
| $\Phi$ | power spectrum of surface pressure fluctuations $\bar{p^2} = \int_0^\infty \Phi(\omega)d\omega$, [pa$^2$/HZ] |
| $P_{ref}$ | reference sound pressure, $2x10^{-5}$ [pa] |
| $x$ | streamwise coordinate, [m] |
| $C_f$ | coefficient of friction, nondimensional |
| $\Phi_0$ | outer variable scaling $\Phi u_\tau/\tau_w^2\delta$, nondimensional |
| $\Phi^+$ | inner variable scaling $\Phi u_\tau^2/\tau_w^2\nu$, nondimensional |
| $\omega$ | angular frequency $2\pi f$, [rad/s] |
| $\omega_0$ | outer variable scaling $\omega\delta/u_\tau$, nondimensional |
| $\omega_+$ | inner variable scaling $\omega\nu/u_\tau^2$, nondimensional |
| $M$ | Mach number $U/c$, nondimensional |
| $c$ | speed of sound, [m/s$^2$] |
| $PSD$ | Power spectral density $10log_{10}(\frac{p^2/[HZ]}{P_{ref}^2})$ [DB] |
| $R_T$ | Timescale $u_\tau\delta/\nu\sqrt{C_f/2}$, nondimensional |

## Appendix A. Tables

**Table A1.** Experiment variables.

| Experiments | $x$ | $\delta$ (mm) | $\theta$ (mm) | $\delta^+$ (mm) | $Re_x$ | $Re_\theta$ | $R_T$ |
|---|---|---|---|---|---|---|---|
| Goody7300w | 3.86 | 39.06 | 4.55 | 6.2 | 6,195,958 | 7300 | 82 |
| Goody23400w | 10.73 | 134.07 | 12.41 | 15.8 | 20,228,285 | 23,400 | 274 |
| Blake8200w | 2.26 | 45.72 | 5.82 | 7.85 | 3,194,738 | 8210 | 95 |
| Blake10200w | 2.69 | 43.18 | 5.79 | 7.24 | 4,736,029 | 10,200 | 104 |
| Blake13200w | 4.12 | 42.93 | 5.74 | 7.19 | 9,341,395 | 13,200 | 119 |
| Gravante2953w | 3.25 | 54.8 | 6.3 | 7.98 | 1,523,373 | 2953 | 42 |
| Gravante4972w | 2.49 | 44.9 | 5 | 6.19 | 2,476,056 | 4972 | 65 |
| Gravante6241 | 3.25 | 53.9 | 6.2 | 7.2 | 3,271,492 | 6241 | 75 |
| Gravante7076w | 3.86 | 62.9 | 7 | 8.25 | 3,901,909 | 7076 | 89 |
| McGrath7010w | 3.52 | 59.53 | 4.9 | 6.58 | 5,046,549 | 7010 | 117 |
| McGrath18820w | 6.51 | 91.04 | 9.44 | 11.88 | 12,975,910 | 18,820 | 208 |
| Farabee3386w | 1.71 | 27.9 | 3.26 | 4.5 | 1,772,915 | 3386 | 47 |
| Farabee4487w | 1.74 | 27.4 | 3.13 | 4.29 | 2,489,277 | 4487 | 60 |
| Farabee6025w | 1.87 | 27.8 | 3.13 | 4.29 | 3,603,538 | 6025 | 77 |
| Schewe1400w | 1.5 | 30 | 3.3 | 4.6 | 622,917 | 1400 | 25 |
| Blitterswyck1866w | 1.1 | 32.6 | 3.5 | 5.1 | 592,743 | 1886 | 35 |
| Blitterswyck2546w | 1.1 | 32.5 | 3.5 | 5 | 800,171 | 2546 | 43 |
| Rackl419848f | 18.9 | 191.27 | 39.14 | 60.1 | 202,736,906 | 419,848 | 1598 |
| Rackl617153f | 32.6 | 327.57 | 57.53 | 88.34 | 349,694,346 | 617,153 | 2544 |
| Rackl823168f | 49.3 | 494.32 | 76.74 | 117.83 | 528,832,248 | 823,168 | 3639 |
| Rocha239216f | 6.7 | 75 | 37.42 | 53.69 | 42,832,000 | 239,216 | 444 |

**Table A1.** *Cont.*

| Experiments | x | $\delta$ (mm) | $\theta$ (mm) | $\delta^+$ (mm) | $Re_x$ | $Re_\theta$ | $R_T$ |
|---|---|---|---|---|---|---|---|
| Rocha151407f | 6.7 | 77 | 24.75 | 37.39 | 40,982,000 | 151,407 | 440 |
| Rocha92037f | 6.7 | 82 | 21.14 | 33.3 | 29,170,000 | 92,037 | 353 |
| Miller12933w | 3 | 50.68 | 5.24 | 6.9 | 7,403,216 | 12,933 | 165 |
| Miller28562w | 3 | 43.77 | 4.29 | 5.52 | 19,963,978 | 28,562 | 328 |
| Miller44899w | 3 | 40.4 | 3.85 | 4.9 | 34,958,975 | 44,899 | 489 |
| Salze1642w | 0.75 | 20.44 | 2.31 | 3.1 | 532,258 | 1642 | 28 |
| Salze5962w | 0.75 | 20.5 | 2.46 | 3.2 | 1,734,375 | 5692 | 67 |
| Salze10687w | 0.75 | 24.97 | 2.75 | 3.6 | 2,916,667 | 10,687 | 117 |

**Table A2.** Experiment variables continued.

| Experiments | v ($\times 10^5$) | M | U | $u_t$ | q | $\tau_w$ | $d^+$ | $C_f$ |
|---|---|---|---|---|---|---|---|---|
| Goody7300w | 1.69 | 0.08 | 27.1 | 0.98 | 399 | 1.04 | 29.5 | 0.0026 |
| Goody23400w | 1.66 | 0.09 | 31.3 | 1.03 | 543 | 1.17 | 31.5 | 0.0022 |
| Blake8200w | 1.58 | 0.07 | 22.3 | 0.85 | 286.6 | 0.84 | 43 | 0.0029 |
| Blake10200w | 1.63 | 0.08 | 28.8 | 1.06 | 462.4 | 1.27 | 51 | 0.0027 |
| Blake13200w | 1.67 | 0.11 | 37.9 | 1.33 | 785.8 | 1.93 | 63 | 0.0025 |
| Gravante2953w | 1.54 | 0.02 | 7.2 | 0.29 | 30.8 | 0.1 | 6 | 0.0033 |
| Gravante4972w | 1.58 | 0.05 | 15.7 | 0.58 | 142.5 | 0.39 | 12.1 | 0.0031 |
| Gravante6241 | 1.56 | 0.05 | 15.7 | 0.57 | 144.2 | 0.38 | 11.9 | 0.0029 |
| Gravante7076w | 1.51 | 0.04 | 15.3 | 0.57 | 141.1 | 1.16 | 11.9 | 0.0028 |
| McGrath7010w | 1.56 | 0.07 | 22.3 | 0.84 | 295 | 0.83 | 27.3 | 0.0027 |
| McGrath18820w | 1.63 | 0.09 | 32.5 | 1.09 | 597.2 | 1.35 | 35.5 | 0.0023 |
| Farabee3386w | 1.49 | 0.05 | 15.5 | 0.62 | 146.9 | 0.48 | 33 | 0.0033 |
| Farabee4487w | 1.49 | 0.06 | 21.3 | 0.83 | 278.5 | 0.85 | 44 | 0.0031 |
| Farabee6025w | 1.47 | 0.08 | 28.3 | 1.07 | 496.9 | 1.43 | 57 | 0.0029 |
| Schewe1400w | 1.51 | 0.02 | 6.3 | 0.28 | 24 | 0.09 | 19 | 0.004 |
| Blitterswyck1866w | 1.41 | 0.02 | 7.6 | 0.34 | 37.4 | 0.15 | 12.1 | 0.004 |
| Blitterswyck2546w | 1.43 | 0.03 | 10.4 | 0.44 | 69 | 0.25 | 15.4 | 0.0038 |
| Rackl419848f | 2.21 | 0.74 | 237.2 | 6.62 | 20,713.1 | 32.26 | 559.7 | 0.0016 |
| Rackl617153f | 2.21 | 0.74 | 237.2 | 6.38 | 20,713.1 | 30 | 539.8 | 0.0014 |
| Rackl823168f | 2.21 | 0.74 | 237.2 | 6.21 | 20,713.1 | 28.43 | 525.5 | 0.0014 |
| Rocha239216f | 2.72 | 0.56 | 174.2 | 5.18 | 8631.4 | 15.27 | 95.1 | 0.0019 |
| Rocha151407f | 3.44 | 0.7 | 210.4 | 6.3 | 9435.3 | 16.92 | 91.6 | 0.002 |
| Rocha92037f | 5.42 | 0.8 | 236.1 | 7.29 | 15,859.1 | 13.93 | 67.2 | 0.0021 |
| Miller12933w | 1.45 | 0.11 | 35.8 | 1.32 | 764.3 | 2.08 | 71.9 | 0.0025 |
| Miller28562w | 1.5 | 0.29 | 99.8 | 3.41 | 5951.6 | 13.91 | 179.8 | 0.0022 |
| Miller44899w | 1.5 | 0.51 | 174.7 | 5.75 | 18,244.6 | 39.47 | 302.8 | 0.002 |
| Salze1642w | 1.55 | 0.03 | 11 | 0.48 | 71.2 | 0.27 | 15.5 | 0.0038 |
| Salze5962w | 1.56 | 0.11 | 36 | 1.35 | 759.7 | 2.14 | 43.4 | 0.0028 |
| Salze10687w | 1.52 | 0.17 | 59 | 2.05 | 2093.7 | 5.06 | 67.6 | 0.0024 |

**Table A3.** Spectrum mean squared error.

| Experiments | Efmitsov | Goody | Goody* | Lagnelli | Lowson | Robertson | Rackl and Weston | Smolyakov |
|---|---|---|---|---|---|---|---|---|
| Goody7300w | 115.7 | 15.9 | 143 | 53.8 | 47.5 | 67.8 | 93 | 4.3 |
| Goody23400w | 74.9 | 3 | 97.5 | 27.3 | 114.1 | 28.1 | 60.3 | 4.1 |
| Blake8200w | 140.5 | 35.6 | 177.7 | 77.7 | 43.7 | 94.8 | 116 | 17.6 |
| Blake10200w | 131.9 | 34.4 | 176 | 77.3 | 66 | 104.7 | 111 | 16.2 |
| Blake13200w | 98.6 | 19.4 | 142.1 | 56 | 80.8 | 82 | 81 | 6.8 |
| Gravante2953w | 136.1 | 33.4 | 191.8 | 46 | 13 | 46.7 | 126.2 | 9.4 |
| Gravante4972w | 77.9 | 6.7 | 102.6 | 37.8 | 21.9 | 51 | 64.7 | 4.7 |
| Gravante6241 | 70.3 | 7 | 95.6 | 27.7 | 19.7 | 39.2 | 58.6 | 5.7 |
| Gravante7076w | 21 | 20.6 | 22 | 24.9 | 99.5 | 30.3 | 8.8 | 61.7 |
| McGrath7010w | 86.7 | 12.1 | 114.3 | 65.7 | 96.2 | 102.1 | 83 | 10.3 |
| McGrath18820w | 93.2 | 10.4 | 114.6 | 69.3 | 102.7 | 104.9 | 87.3 | 7.6 |
| Farabee3386w | 216.3 | 16.9 | 124.5 | 184.3 | 199.3 | 275.8 | 205.4 | 101.6 |

**Table A3.** *Cont.*

| Experiments | Efmitsov | Goody | Goody* | Lagnelli | Lowson | Robertson | Rackl and Weston | Smolyakov |
|---|---|---|---|---|---|---|---|---|
| Farabee4487w | 203.5 | 14.9 | 111.4 | 175.2 | 184.2 | 262.6 | 187.7 | 116.7 |
| Farabee6025w | 201.5 | 7.6 | 82.5 | 184.7 | 215.7 | 281.3 | 190.4 | 141 |
| Schewe1400w | 56.6 | 5 | 103.7 | 20.9 | 19.1 | 27.7 | 61.1 | 6.8 |
| Blitterswyck1866w | 99.7 | 20.3 | 134.4 | 58.1 | 26.9 | 59.2 | 89.8 | 12.3 |
| Blitterswyck2546w | 101.6 | 28.7 | 147.4 | 52.2 | 31.5 | 55.4 | 93.1 | 22.3 |
| Rackl419848f | 8.1 | 117.1 | 12.2 | 234.1 | 41 | 25.8 | 7.5 | 201.1 |
| Rackl617153f | 6.5 | 98 | 8.9 | 467 | 71.8 | 33.3 | 5.4 | 148.5 |
| Rackl823168f | 8.7 | 102.3 | 9.1 | 781.3 | 99.7 | 33.9 | 6.8 | 137.4 |
| Rocha239216f | 4.5 | 27.4 | 9.9 | 5.7 | 20.2 | 18.7 | 5.6 | 37 |
| Rocha151407f | 4.4 | 71.5 | 0.6 | 21.1 | 3.6 | 7.3 | 2.4 | 93.3 |
| Rocha92037f | 16.1 | 110.3 | 6.4 | 56.1 | 4.1 | 8.8 | 11.4 | 145.5 |
| Miller12933w | 65.9 | 3.9 | 102 | 53.7 | 71.3 | 68.1 | 70.6 | 1.5 |
| Miller28562w | 60.4 | 1.8 | 83.1 | 87.9 | 123.8 | 138.9 | 62.6 | 19.8 |
| Miller44899w | 60.5 | 1.5 | 65.3 | 98.8 | 138.2 | 170.3 | 59.2 | 52.6 |
| Salze1642w | 66.2 | 9.1 | 121.7 | 22.8 | 20.6 | 27.8 | 62.9 | 5.2 |
| Salze5962w | 61.2 | 4.9 | 104.8 | 27 | 38.2 | 42.6 | 47.3 | 10.9 |
| Salze10687w | 61.7 | 5.9 | 105 | 29.1 | 45.1 | 44.8 | 45.4 | 12.1 |
| Averages | 81 | 29.2 | 93.4 | 107.7 | 71 | 80.5 | 72.6 | 48.7 |

**Table A4.** Spectrum mean squared error for the low frequency range.

| Experiments | Efimtsov | Goody | Lagnelli | Lowson | Robertson | Rackl and Weston | Smolyakov |
|---|---|---|---|---|---|---|---|
| McGrath7010w | 321.2 | 69 | 347.3 | 424 | 534 | 320.7 | 21.6 |
| McGrath18820w | 295.3 | 47.6 | 360.8 | 439.6 | 552.8 | 294.8 | 26.8 |
| Farabee3386w | 401.5 | 5.8 | 382 | 459 | 584.9 | 401.4 | 234.5 |
| Farabee4487w | 365.9 | 1 | 361.2 | 435.3 | 557.7 | 365.7 | 287.8 |
| Farabee6025w | 396.1 | 3.3 | 406.3 | 483.7 | 612.4 | 395.9 | 331.4 |
| Miller44899w | 78.2 | 7.3 | 129.1 | 172.9 | 255.9 | 75.8 | 213.9 |

**Table A5.** Spectrum mean squared error for the medium frequency range.

| Experiments | Efimtsov | Goody | Lagnelli | Lowson | Robertson | Rackl and Weston | Smolyakov |
|---|---|---|---|---|---|---|---|
| Goody7300w | 48 | 1.9 | 52 | 76.9 | 58 | 72.5 | 2 |
| Goody23400w | 25.7 | 0.8 | 50.5 | 79.8 | 72.7 | 36.4 | 6.3 |
| Blake8200w | 54.1 | 5.9 | 53.9 | 83.9 | 81.9 | 67.6 | 0.7 |
| Blake10200w | 76 | 12.2 | 86.5 | 125 | 143.5 | 80.3 | 3.3 |
| Blake13200w | 74.4 | 9.9 | 98.5 | 139 | 152.5 | 80.5 | 2.1 |
| Gravante2953w | 53.9 | 4.6 | 35.6 | 56.5 | 37.1 | 93.8 | 0.5 |
| Gravante4972w | 27.3 | 1.3 | 23.7 | 43.9 | 41.8 | 40.7 | 10.9 |
| Gravante6241 | 18.9 | 1.3 | 18.3 | 36.5 | 34.6 | 30.4 | 13 |
| Gravante7076w | 4.9 | 52.1 | 3.5 | 0 | 1 | 4.1 | 151 |
| McGrath7010w | 68.2 | 9.1 | 77.8 | 112.6 | 137.6 | 73.2 | 15.8 |
| McGrath18820w | 77.9 | 9.1 | 109.3 | 151.2 | 186.3 | 80.4 | 15.7 |
| Farabee3386w | 61.1 | 4.5 | 50.5 | 79.7 | 99.2 | 70.4 | 40.1 |
| Farabee4487w | 57.2 | 3.3 | 53.4 | 84.3 | 106.1 | 63.5 | 42.7 |
| Farabee6025w | 57.2 | 2.2 | 59.7 | 92.3 | 118.4 | 61.1 | 49.6 |
| Schewe1400w | 38 | 3.1 | 16.9 | 34.8 | 34.2 | 57.7 | 11.5 |
| Blitterswyck1866w | 16 | 0.4 | 3 | 11.7 | 6.9 | 35.4 | 16 |
| Blitterswyck2546w | 19.7 | 0.2 | 7.4 | 20.5 | 20.8 | 31.1 | 21 |
| Rackl419848f | 12.2 | 134.2 | 20.9 | 11.3 | 21.8 | 11.9 | 301.9 |
| Rackl617153f | 11.8 | 111 | 59 | 30 | 38.8 | 11.5 | 226.9 |
| Rackl823168f | 17.8 | 122.2 | 153 | 31.5 | 35.7 | 17.5 | 217.1 |
| Rocha239216f | 2 | 30.8 | 7.9 | 27.1 | 31.1 | 1.7 | 52.1 |
| Rocha151407f | 5.7 | 72.8 | 6.9 | 4.6 | 8.5 | 3.4 | 107.9 |
| Rocha92037f | 20.7 | 117.3 | 31.2 | 3 | 5.4 | 15.5 | 171.4 |
| Miller12933w | 55.7 | 5.2 | 69.8 | 104.5 | 111.5 | 61.2 | 1.7 |
| Miller28562w | 64.4 | 2.4 | 100.2 | 141 | 173.9 | 62 | 28 |
| Miller44899w | 60.1 | 0.9 | 100.8 | 140.4 | 173.6 | 57.2 | 39.8 |
| Salze1642w | 39 | 3.9 | 16.6 | 34.5 | 34.6 | 54.8 | 10.7 |
| Salze5962w | 50.6 | 4 | 42.6 | 70.5 | 88.2 | 49.9 | 27.8 |
| Salze10687w | 47 | 2 | 47.1 | 76.3 | 101.1 | 40.9 | 36.6 |

**Table A6.** Spectrum mean squared error for the overlap frequency range.

| Experiments | Efimtsov | Goody | Lagnelli | Lowson | Robertson | Rackl and Weston | Smolyakov |
|---|---|---|---|---|---|---|---|
| Goody7300w | 86.7 | 5.3 | 48.3 | 49.3 | 34.3 | 98.8 | 3.3 |
| Goody23400w | 85.4 | 3.3 | 32.7 | 46.5 | 27.4 | 84.7 | 1.2 |
| Blake8200w | 63.5 | 2.2 | 28.2 | 33.2 | 21.3 | 73.2 | 0.4 |
| Blake10200w | 75.5 | 4 | 36 | 39.4 | 28.3 | 80.8 | 1.3 |
| Blake13200w | 75.3 | 1.8 | 19.6 | 25.3 | 16 | 63 | 1.2 |
| Gravante2953w | 77.5 | 6.2 | 25.9 | 28 | 16.6 | 96.4 | 2.2 |
| Gravante4972w | 46.1 | 0.5 | 11.6 | 13.5 | 6.9 | 53.8 | 0.9 |
| Gravante6241 | 45.5 | 0.5 | 9.3 | 10.6 | 5.2 | 50.3 | 1.6 |
| Gravante7076w | 0.7 | 42.8 | 17.3 | 32.2 | 25.8 | 0.8 | 59.5 |
| McGrath7010w | 55.9 | 0.8 | 25.4 | 31.6 | 17.9 | 68.5 | 0.2 |
| McGrath18820w | 83.4 | 4.6 | 30.8 | 42.6 | 26.1 | 81.5 | 0.6 |
| Farabee3386w | 59.8 | 1.1 | 8.7 | 5.7 | 3.2 | 54.7 | 0.1 |
| Farabee4487w | 56.7 | 0.8 | 13.6 | 15.3 | 8.4 | 55.2 | 0.2 |
| Farabee6025w | 56 | 0.4 | 11.3 | 15.6 | 7.4 | 46.2 | 1.4 |
| Schewe1400w | 40.2 | 0.7 | 8.3 | 14.6 | 4 | 63.4 | 0.3 |
| Blitterswyck1866w | 24.5 | 0.2 | 2.1 | 6.1 | 0.8 | 41.6 | 4 |
| Blitterswyck2546w | 44.7 | 1 | 8.8 | 13.1 | 4.1 | 57.7 | 0.3 |
| Rackl419848f | 4.1 | 99.9 | 447.3 | 70.6 | 29.7 | 3.2 | 100.2 |
| Rackl617153f | 2.5 | 88.5 | 766.1 | 102.4 | 29.2 | 0.9 | 91 |
| Rackl823168f | 3.8 | 91.7 | 1114 | 135.7 | 33 | 1.2 | 95.2 |
| Rocha239216f | 7.3 | 23.6 | 3.3 | 12.5 | 4.9 | 9.9 | 20.2 |
| Rocha151407f | 1.6 | 68.7 | 51.9 | 1.5 | 4.7 | 0.2 | 61.7 |
| Rocha92037f | 6.3 | 95.3 | 110 | 6.6 | 16.2 | 2.3 | 89.5 |
| Miller12933w | 75.1 | 2.8 | 39.2 | 41.5 | 29 | 79.1 | 1.3 |
| Miller28562w | 51.3 | 0.6 | 59.2 | 83.6 | 57.3 | 64.1 | 0.9 |
| Miller44899w | 46.1 | 0 | 51.9 | 85.5 | 56.2 | 60.3 | 0.4 |
| Salze1642w | 47.6 | 2 | 9.6 | 15.2 | 4.7 | 60.2 | 0 |
| Salze5962w | 56.6 | 2.5 | 24.3 | 33.9 | 20.4 | 57.6 | 0.4 |
| Salze10687w | 57.8 | 2.3 | 29.8 | 41 | 27.4 | 52.7 | 0.9 |

**Table A7.** Spectrum mean squared error for the high frequency range.

| Experiments | Efimtsov | Goody | Lagnelli | Lowson | Robertson | Rackl and Weston | Smolyakov |
|---|---|---|---|---|---|---|---|
| Goody7300w | 164.4 | 27.9 | 57 | 30.7 | 86.5 | 102 | 6 |
| Goody23400w | 74 | 3.3 | 14.7 | 207.2 | 17.8 | 35.7 | 7.2 |
| Blake8200w | 244.9 | 76.4 | 126.7 | 28.3 | 154.6 | 174.2 | 39.6 |
| Blake10200w | 252.3 | 90.3 | 107.9 | 25.2 | 136.9 | 176.5 | 45.7 |
| Blake13200w | 158.1 | 51.1 | 28.5 | 49 | 42.3 | 99.7 | 19.4 |
| Gravante2953w | 157.2 | 42.6 | 52 | 6.1 | 55.3 | 136.2 | 11.9 |
| Gravante4972w | 126.2 | 12.8 | 57.5 | 9 | 73.8 | 86.1 | 1.5 |
| Gravante6241 | 124 | 15 | 44.5 | 10.7 | 59.8 | 85.4 | 2 |
| Gravante7076w | 25.6 | 14.9 | 27.5 | 117.2 | 32.8 | 10.5 | 56.8 |
| McGrath7010w | 89.1 | 14 | 16 | 52.2 | 20.8 | 54.1 | 8.7 |
| McGrath18820w | 120.7 | 24 | 1.2 | 68.6 | 4.5 | 75.5 | 1.5 |
| Farabee3386w | 193 | 49.1 | 123.1 | 43.8 | 140.5 | 142.6 | 22.7 |
| Farabee4487w | 197.9 | 47.1 | 124.8 | 39.9 | 148.5 | 138.5 | 24.2 |
| Farabee6025w | 144.3 | 28.4 | 71.1 | 32.9 | 89.7 | 90.8 | 14.2 |
| Schewe1400w | 74.9 | 7.3 | 25.9 | 5.9 | 25 | 63.8 | 3.6 |
| Blitterswyck1866w | 139.8 | 30.3 | 85.8 | 35.6 | 86.5 | 115.8 | 12.8 |
| Blitterswyck2546w | 191.5 | 63.9 | 107.5 | 49.1 | 107 | 157.3 | 34.2 |
| Salze1642w | 99.5 | 16.6 | 33.5 | 8.4 | 28.7 | 71.9 | 1.4 |
| Salze5962w | 76 | 8 | 13.8 | 9.6 | 17 | 35.4 | 3.3 |
| Salze10687w | 85.4 | 16.5 | 7.4 | 16.7 | 10.3 | 38.2 | 3.4 |

## Appendix B. Auxiliary Functions

For Tables A3–A7, the different frequency response models were predicted starting with only the Mach number, the stream-wise location, the pressure, and the temperature, to provide a fair comparison of the different models. The predicted boundary layer parameters are close to the measured parameters causing minimal impact on the ability

of each model to predict the experimental results. The following equations were used to determine important inputs for the frequency response models [8]

$$C_f = 0.37(log_{10}Re_x)^{-2.584} \tag{A1}$$

Two different equations exist for the prediction of the boundary layer thickness, Equation (A2) is the US method, and Equation (A3) is the Russian method. The US method generally predicts a marginally larger boundary layer thickness [11].

$$\delta = 0.37xRe_x^{-\frac{1}{5}}[1 + (\frac{Re_x}{6.9x10^7})]^{0.35} \tag{A2}$$

$$\delta = 0.37xRe_x^{-\frac{1}{5}}[1 + 0.144M^2]^{0.35} \tag{A3}$$

Two different equations exist for the prediction of the displacement thickness, Equation (A4) is the US method, and Equation (A5) is the Russian method. The US method generally predicts a marginally larger displacement thickness [11].

$$\delta^* = \frac{\delta(1.3 + 0.43M^2)}{10.4 + 0.5M^2(1 + 2x10^{-8})^{0.333}} \tag{A4}$$

$$\delta^* = \delta|(1 - \frac{1.88(log_{10}Re_x - 3.06)}{(1.88log_{10}Re_x - 4.52)(1 + 0.065M^2)}| \tag{A5}$$

The momentum thickness is defined in equation A6 [11].

$$\theta = \frac{\delta}{10.4 + 0.5M^2(1 + 2*10^{-8})^{0.333}} \tag{A6}$$

The ratio of the outer-layer-to-inner-layer timescale is defined in Equation (A7) [19].

$$R_\tau = (\frac{u_\tau\delta}{\nu})\sqrt{\frac{C_f}{2}} \tag{A7}$$

## References

1. Bull, M. Wall-Pressure fluctuationa beneath turbulent boundary layers: Some reflections in forty years of research. *J. Sound Vib.* **1995**, *190*, 299–315. [CrossRef]
2. Mellert, V.; Baumann, I.; Freese, N.; Weber, R. Impact of sound and vibration on health, travel comfort and performance of flight attendants and pilots. *Aerosp. Sci. Technol.* **2008**, *12*, 18–25. [CrossRef]
3. Wilby, J. Aircraft Interior Noise. *J. Sound Vib.* **1996**, *190*, 545–564. [CrossRef]
4. Willmarth, W.; Wooldridge, C. Measurements of the fluctuating pressure at the wall beneath a thick turbulent boundary layer. *J. Fluid Mech.* **1962**, *1962*, 187–210. [CrossRef]
5. Bull, M. On the form of the wall-pressure spectrum in a turbulent boundary layer in relation to noise generation by boundary layer-surface interactions. In *Mechanics of Sound Generation in Flows, Proceedings of the Joint Symposium, Goettingen, West Germany*; Springer: Berlin, Germany, 1979.
6. Blitterswyk, J.V. Experimental Characterization of Turbulent Motions Using Wall-Pressure Measurements in Low Reynolds Number Turbulent Bondary Laters. Master's Thesis, Carleton University, Ottawa, ON, Canada, 2016; doi:10.22215/etd/2016-11667. [CrossRef]
7. Goody, M.C.; Simpson, L. Surface Pressure Fluctuations Beneath Two and Three Dimensional Turbulent Boundary Layers. *AIAA J.* **2000**, *38*. [CrossRef]
8. Blitterswyk, J.V.; Rocha, J. Prediction and Measurement of flow induced wall presure fluctuations at low Mach numbers. *J. Can. Acoust.* **2014**, *42*, 3–14.
9. Miller, T.S. *Turbulent Boundary Layer Models for Acoustic Analysis*; Wichita State University: Wichita, KS, USA, 2011.
10. Salze, E.; Bailly, C.; Marsden, O.; Jondeau, E.; Juve, D. An experimental characterization of wall pressure wavevector-frequency spectra in the presence of pressure gradients. In Proceedings of the 20th AIAA/CEAS Aeroacoustics Conference, Atlanta, GA, USA, 16–20 June 2014. [CrossRef]
11. Rizzi, S.A.; Rackl, R.G.; Andrianov, E.V. *Flight Test Measurements From The TU-144LL Structure/Cabin Noise Experiment*; TM-2000-209858; NASA: Hampton, VA, USA, 2000.

12. Rocha, J.; Palumbo, D. On the sensitivity of sound power radiated by aircraft panels to turbulent boundary layer parameters. *J. Sound Vib.* **2012**, *331*. [CrossRef]

13. Efimtsov, B.; Kozlov, N.; Kravchenko, S.; Anderson, A. Wall Pressure-Fluctuation Spectra at Small Forward-Facing Steps. In Proceedings of the 5th AIAA/CEAS Aeroacoustics Conference and Exhibit, Bellevue, WA, USA, 10–12 May 1999.

14. Efimtsov, B. Similarity criteria for the spectra of wall pressure fluctuations in a turbulent boundary layer. *Akust. Zhurnal* **1984**, *30*, 58–61.

15. Rackl, R.; Weston, A. *Modeling of Turbulent Boundary Layer Surface Pressure Fluctuation Auto and Cross Spectra-Verification and Adjustments Based on TU-144LL Data*; CR-2005-213938; NASA: Washington, DC, USA, 2005.

16. Lowson, M. *Prediction of Boundary Layer Pressure Fluctuations*; Wyle Laboratories: Wright-Patterson Air Force Base, OH 1968.

17. Robertson, J. *Prediction of in Flight Fluctuating Pressure Environments Including Protuberance Induced Flow*; Wyle Laboratories: Huntsville, AL, USA, 1971.

18. Lagnelli, A.; Wolfe, H. Prediction of FLuctuating Pressure in Attached and Separated Turbulent Boundary-Layer Flow. *J. Aircr.* **1993**, *30*, 962–970. [CrossRef]

19. Goody, M. Empirical spectral model of surface pressure fluctuations. *AIAA J.* **2004**, *42*, 1788–1794. [CrossRef]

20. Smol'yakov, A. Calculation of the Spectra of Pseudosound Wall Pressure Fluctuations in Turbulent Boundary Layers. *Acoust. Phys.* **2000**, *26*, 342–347. [CrossRef]

21. Hwang, Y.; Bonnes, W.K.; Hambric, S.A. Comparison of Semi Empirical Models for turbulent boundary layer wall pressure spectra. *J. Sound Vib.* **2009**, *319*, 199–217. [CrossRef]

22. Schewe, G. On the structure and resolution of wall-pressure fluctuations assoiciated with turbulent boundary-layer flow. *J. Fluid Mech.* **1983**, *134*. [CrossRef]

23. Blake, W.K. Turbulent boundary-layer wall-presure fluctuations on smooth and rough walls. *J. Fluid Mech.* **1970**, *44*, 637–660. [CrossRef]

24. Farabee, T.M.; Casarella, M.J. Spectral features of wall pressure fluctuations beneath turblent boundary layers. *Phys. Fluids A Fluid Dyn.* **1991**, *3*, 2410–2420. [CrossRef]

25. McGrath, B.; Simpson, R. *Some Features of Surface Pressure Fluctuations in Turbulent Boundary Layers with Zero and Favourable Pressure Gradients*; CR-4051; NASA: Washington, DC, USA, 1987.

26. Gravante, S.; Naguib, A.; Wark, C.; Nagib, M. Characterization of the pressure Fluctuations Under a Fully Developed Turbulent Booundary Layer. *AIAA J.* **1998**, *36*, 1808–1816. [CrossRef]

27. Eckel, A.; Istvan, V. Design and construction considerations for automotive and aautomotive component acoustic test facilities. In Proceedings of the International Congress and Exposition on Noise Control Engineering, Dearborn, MI, USA, 19–21 August 2002.

28. Naguib, A.M.; Gravante, S.P.; Wark, C.E. Extraction of Turbulent wall-pressure time series using an optimal filtering scheme. *Exp. Fluids* **1996**, *22*, 14–22. [CrossRef]

29. Simpson, R.L.; M., G.; McGrath, B.E. Surface pressure fluctuations in a separating turbulent boundary layer. *J. Fluid Mech.* **1986**, *177*, 167–186. [CrossRef]

30. Geib, F.E. Measurements on the Effect of the Transducer Size on the Resolution of Boundary-Leyer Pressure Fluctuations. *J. Acoust. Soc. Am.* **1968**, *46*, 253–261. [CrossRef]

31. Corcos, G.M. Resolution of Pressure in Turbulence. *J. Acoust. Soc. Am.* **1963**, *35*, 192–199. [CrossRef]

32. Chase, D. Modeling the Wavevector-Frequency Spectrum of Turbulent Boundary Layer Wall Pressure. *J. Sound Vib.* **1980**, *70*, 29–67. [CrossRef]

33. Howe, M.S. *Acoustics of Fluid-Structure Interactions*; Cambridge University Press: Cambridge, UK, 1998.

34. Olivero-Bally, P.; Forestier, B.; Focquency, E.; Olvero, P. Wall Pressure Fluctuations in Natural and Manipulated Turbulent Boundary Layers in Air and Water. *Am. Soc. Mechanocal Eng.* **1993**, *168*, 63–74.